Chemical Science

ROYAL SOCIETY OF CHEMISTRY

EDGE ARTICLE

View Article Online
View Journal | View Issue

Cite this: *Chem. Sci.*, 2023, **14**, 4935

All publication charges for this article have been paid for by the Royal Society of Chemistry

Received 12th January 2023
Accepted 2nd April 2023

DOI: 10.1039/d3sc00231d

rsc.li/chemical-science

Mismatched covalent and noncovalent templating leads to large coiled coil-templated macrocycles†

Kyla J. Stingley,‡ Benjamin A. Carpenter,‡ Kelsey M. Kean‡ and Marcey L. Waters *

Herein we describe the use of dynamic combinatorial chemistry to self-assemble complex coiled coil motifs. We amide-coupled a series of peptides designed to form homodimeric coiled coils with 3,5-dithiobenzoic acid (**B**) at the N-terminus and then allowed each **B**-peptide to undergo disulfide exchange. In the absence of peptide, monomer **B** forms cyclic trimers and tetramers, and thus we expected that addition of the peptide to monomer **B** would shift the equilibrium towards the tetramer to maximize coiled coil formation. Unexpectedly, we found that internal templation of the **B**-peptide through coiled coil formation shifts the equilibrium towards larger macrocycles up to 13 **B**-peptide subunits, with a preference for 4, 7, and 10-membered macrocycles. These macrocyclic assemblies display greater helicity and thermal stability relative to intermolecular coiled coil homodimer controls. The preference for large macrocycles is driven by the strength of the coiled coil, as increasing the coiled coil affinity increases the fraction of larger macrocycles. This system represents a new approach towards the development of complex peptide and protein assemblies.

Introduction

Proteins form a complex array of self-assembled structures, ranging from discrete structures such as homo- or heterodimers to extended assemblies such as the protein filaments, keratin, myosin, and others. *De novo* protein design has provided insight into the factors that drive protein assemblies, including discrete α-helical coiled coil[1–8] and β-sheet assemblies.[9–11] Higher order supramolecular assemblies of peptides that are driven by covalent linkage, metal templation, and noncovalent assembly, which result in the formation of complex 1-, 2- and 3D assemblies with interesting materials properties, have also been investigated.[6,8,12–26]

The coupling of dynamic combinatorial chemistry (DCC)[27] with noncovalent peptide assembly is complementary to *de novo* design as it allows for the discovery of new, often unexpected assemblies and properties. DCC utilizes building blocks that can reversibly react with one another *via* covalent bond formation to produce a dynamic combinatorial library (DCL) whose speciation is controlled by thermodynamic stability.[27] The introduction of peptide components to a DCC system couples covalent bond formation with noncovalent assembly to create new and often unanticipated structures. We and others have previously reported using this approach to create novel structures.[28–41] Among these, globular-like assemblies have been discovered by coupling β-turns,[28,29,31] and nucleobases, with DCC while fibril formation has also been observed with short unstructured peptides and β-strand-templated DCLs *via* nonspecific hydrophobic interactions and β-sheet assembly, respectively.[32–37] However, the coupling of DCC with peptides that are designed to form discrete *quaternary* structures has only been minimally explored.[38,39,42] To this end, we sought to investigate how the coupling of a DCC building block to a peptide that favors a discrete quaternary structure influences the balance between formation of covalent bonds between DCC monomers and noncovalent interactions between peptides to give biomimetic peptide assemblies. Herein, we describe the coupling of a series of peptides, which are designed to form homodimeric α-helical coiled coils, with a DCC building block that favors cyclic trimer and tetramer formation *via* reversible covalent bond formation (Fig. 1a). When combined, these two mismatched components, with competing driving forces to form noncovalent dimers *versus* covalent trimers and tetramers, create a new class of oligomeric macrocyclic peptide assemblies (Fig. 1). Since the coiled coil sequences favor dimerization and the covalent subunit prefers trimeric and tetrameric species, it would be reasonable to expect both factors to shift the equilibrium speciation toward the tetrameric species due to the creation of two coiled coils (Fig. 1d). However, we find the interplay between the covalent and noncovalent interactions also gives rise to significant amounts of larger cyclic oligomers, overcoming the inherent entropic preference for smaller macrocycles (Fig. 1e). These assemblies represent a middle ground between uncontrolled aggregates and defined protein

Department of Chemistry, University of North Carolina at Chapel Hill, CB 3290, Chapel Hill, NC 27599, USA. E-mail: mlwaters@email.unc.edu

† Electronic supplementary information (ESI) available: Additional experimental details, LC-MS and MALDI methods and data, SDS-PAGE procedures and data, and CD conditions and data. See DOI: https://doi.org/10.1039/d3sc00231d

‡ These authors contributed equally.

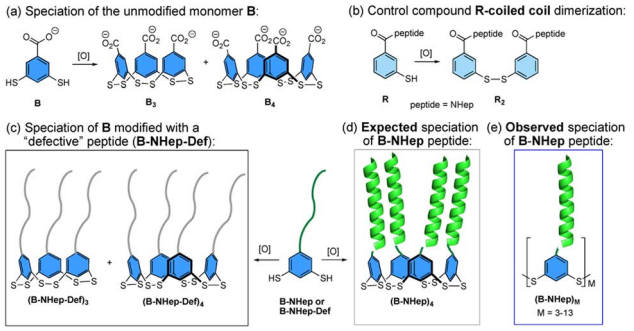

Fig. 1 Cartoon depiction of the (a) speciation of unmodified monomer **B** in a dynamic combinatorial library (DCL). (b) Structure and dimerization of control monomer **R**. (c) Speciation of **B-*N*Hep-Def** monomers; (d) and (e) **Expected** and **Observed** speciation of the DCL of **B-*N*Hep** libraries.

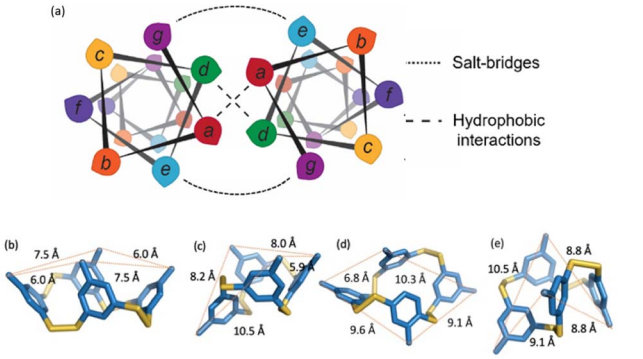

Fig. 2 (a) Helical wheel diagram depicting the coiled coil interface and location of each amino acid position in the heptad. (b–e) Computational models of possible conformations of B_4 showing distances between neighboring carbonyl carbons. (b) "All up", corresponding to the orientation in Fig. 1; (c), "1 down"; (d) "1,2-down"; (e) "1,3-alternating".

assemblies, expanding the scope of peptidic complexity of other reported systems.[12,33] We find that the shift in equilibrium to larger macrocycles is directly linked to the stability of the coiled coil and that specific macrocyclic ring sizes are favored over others. These findings demonstrate the interplay of effective molarity, binding energy, and degeneracy that give rise to emergent behavior that mimics the factors that contribute to complex biological assemblies.

Results

System design

The monomer design couples a DCC building block with a peptide designed to form a homodimeric coiled coil with the expectation that speciation of the library and formation of the coiled coil would be energetically coupled, resulting in novel protein-like assemblies (Fig. 1). We chose to use 3,5-dithiobenzoic acid, **B**, as the DCC building block capable of forming reversible covalent bonds.[40] This building block has been utilized previously in studies where peptides have been coupled to the **B** subunit *via* amide coupling.[33,36,40] The two thiol groups of **B** allow for disulfide formation in atmospheric oxygen, and equilibrium is subsequently reached *via* thiol–disulfide exchange. Libraries were generated by adding desired monomer in 50 mM borate buffer (pH 8.4) and equilibrating at room temperature for at least 7 days before analysis. Each library was prepared at 150 μM total monomer concentration unless otherwise noted; the concentration of monomer stocks was determined *via* absorbance (Fig. S1†). Under similar conditions, libraries of unmodified **B** have been shown to almost exclusively favor trimeric and tetrameric macrocycles (Fig. 1a), as larger rings are entropically less favorable.[36,40] As a control, we also investigated an analog of **B**, 3-thiobenzoic acid, dubbed monomer **R**, which only contains a single thiol (Fig. 1b). Thus, libraries of **R** will only form dimeric species and function as a control for the influence of covalent bond formation on effective molarity and coiled coil formation.

Homodimeric coiled coil peptide sequences were chosen based on previously described sequence design from the Woolfson group.[2–5,7] Each peptide consists of heptad repeats with hydrophobic residues at the *a* and *d* position to create the dimerization interface (Fig. 2a). The placement of Ile (I) at the *a* positions and Leu (L) at the *d* positions, in addition to a single Asn (N) residue at one *a* position, has been shown to specify parallel dimerization due to "knobs-into-holes" packing of the hydrophobic interface coupled with buried hydrogen bonding of the Asn residues between two peptides.[2–4] Placing Arg (R) at the *e* position and Glu (E) at the *g* position favors homodimerization through complementary electrostatic interactions.[3,4] The remaining *b*, *c*, and *f* positions, which do not participate in these noncovalent interactions, were respectively populated with Ala (A) residues to improve helicity, Glu to increase water solubility, or Trp (W) for concentration determination. A Gly (G) spacer on the N-terminus was incorporated between the DCC building block **B** and the peptide. Structural analysis of distances between the *a* positions at the N-termini of a coiled coil (7.5 Å) as well as computational analysis of the distance between the carbonyl carbon position in the B_4 macrocycles (ranging from 5.9–10.5 Å, depending on the conformation) suggests that a single Gly spacer is sufficient to allow coiled coil formation within the macrocycles, although not all conformations orient the peptides in the same direction (Fig. 2b–e).

Previous reports have shown that *de novo* coiled coil peptides exhibit length dependent affinity; 4-heptad peptides exhibit low nanomolar affinity, 3-heptad peptides exhibit low micromolar affinity, and so on.[2,3,43] Thus, we utilized a series of peptide sequences coupled to monomer **B** that range from 1.5-heptad to 3-heptad in length, referred to as **B-*N*Hep** where *N* is the number of heptads, to systematically vary the strength of the coiled coil (Table 1, Fig. S2–S5†). In doing so, we were able to vary the relative energetic contribution of the coiled coil formation *versus* the covalent DCC linkage on the speciation preference of the library. Acetyl-capped peptides (**Ac-*N*Hep**) were used as controls to evaluate the extent of folding in the absence of covalent interactions from the DCC building blocks (Fig. S6–S9†). The 2.5 and 3-heptad peptide were also coupled to

Table 1 Sequences of peptides used in these studies. *N*Hep represents the number of heptads and Def represents defective sequences. *X* is representative of an acetyl group (Ac), monomer **B**, or monomer **R**

Peptide	Sequence X-G-gabcdef-gabcdef-gabcdef-NH_2
X-1.5Hep	X-G-EIAALRE-ENAW-NH_2
X-2Hep	X-G-EIAALRE-ENAALRW-NH_2
X-2Hep-Def	X-G-EIAAGRE-ENAAGRW-NH_2
X-2.5Hep	X-G-EIAALRE-ENAALRW-EIA-NH_2
X-2.5Hep-Def	X-G-EIAAGRE-ENAAGRW-EIA-NH_2
X-3Hep	X-G-EIAALRE-ENAALRW-EIAALRE-NH_2

building block **R** to determine the impact of a single covalent linker on folding (Fig. S10 and S11†). Lastly, we synthesized a set of defective peptides (**Ac-*N*Hep-Def** and **B-*N*Hep-Def**) that cannot form a coiled coil (Fig. S12–S15†) by replacing the Leu residues at the *d* positions of each heptad with Gly (G; Table 1). Below we describe the characterization of the speciation of these DCLs by mass spectrometry and SDS-PAGE electrophoresis, as well as the characterization of folding and stability by circular dichroism (CD) spectroscopy.

Characterization of speciation by LC-MS and MALDI-TOF MS

To assess the influence of each peptide on speciation of the DCL, we utilized LC-MS analysis to compare speciation of the **B-*N*Hep** libraries to the parent **B** monomer alone. The parent compound **B** exhibits two peaks representing $\mathbf{B_3}$ and $\mathbf{B_4}$ with $\mathbf{B_3}$ as the major species, as has been observed previously (Fig. S16†).[36,40] Similarly the single-thiol monomer **R** behaved as expected, forming exclusively $\mathbf{R_2}$ (Fig. S17†). Because the peptide sequences favor coiled coil dimer formation in a length-dependent manner, we expected that the appended peptide would shift the library toward tetramer, allowing for the formation of two coiled coils per macrocycle, and that the shift towards $\mathbf{B_4}$ would correlate with increasing peptide length. Analysis of the **B-1.5Hep** library indicates the formation of $\mathbf{B_3}$ and $\mathbf{B_4}$ with $\mathbf{B_3}$ as the major species (Fig. S18†), similar to **B** alone. This suggests that the 1.5Hep peptide is too short to form significantly stabilizing coiled coils that would perturb the equilibrium, even when in a covalent complex. However, while **B-2Hep**, **B-2.5Hep**, and **B-3Hep** also form $\mathbf{B_3}$ and $\mathbf{B_4}$ with a shift towards $\mathbf{B_4}$ as expected, additional broad peaks that did not ionize well are also observed (Fig. S19–S21†). Attempts to optimize the chromatography did not improve the peak resolution, and the species giving rise to these peaks did not ionize well by ESI-MS. In contrast, the defective **B**-peptide conjugates, **B-2Hep-Def** and **B-2.5Hep-Def** form only $\mathbf{B_3}$ and $\mathbf{B_4}$, similar to **B-1.5Hep** and **B** alone (Fig. S22 and S23†), suggesting that the broad peaks are not solely due to peptide length but correlate with the ability to form a coiled coil. Further, **R-2.5Hep** and **R-2.5Hep-Def** libraries showed only the expected peaks for covalent dimers, suggesting that the unidentified species are not noncovalent aggregates (Fig. S24 and S25†). Based on these data and the size of some species reported in related systems,[32,35] these unidentifiable masses were hypothesized to be large oligomers or assemblies.

To further characterize the speciation of the libraries, we analyzed DCLs of **B-1.5Hep-3Hep** and **B-2.5Hep-Def** by MALDI-TOF mass spectrometry using at least 20-fold higher concentration libraries to observe higher mass species (3–8 mM, Fig. S26–S30†). We also utilized a relatively high laser intensity to observe higher mass species, sacrificing resolution, such that the isotopic envelopes were not resolved.[17] Analysis of the peak maxima, representing the isotope average mass, demonstrate a difference of a single **B-*N*Hep** unit between each peak (Tables S2–S6†). This analysis indicates that **B-2Hep**, **B-2.5Hep**, and **B-3Hep** all show masses up to at least $\mathbf{B_{11}}$, indicating that large oligomers are formed in these DCLs. By contrast, **B-2.5Hep-Def** only shows species up to $\mathbf{B_7}$, suggesting the importance of coiled coil formation in forming higher mass species. As only $\mathbf{B_3}$ and $\mathbf{B_4}$ were observed by LC-MS in the **B-2.5Hep-Def** library (Fig. S23†), the presence of some amount of $\mathbf{B_5}$–$\mathbf{B_7}$ in the MALDI data may be due to the much higher concentrations of these experiments. While analysis through MALDI provided evidence for the formation of higher order oligomers, it did not provide reliable information regarding relative abundance. Thus, we turned to gel electrophoresis to gain further insight into the speciation of these libraries.

Coiled coils shift the equilibrium to higher mass species as observed by SDS-PAGE analysis

To investigate the higher mass species, we used Bis-Tris SDS-PAGE to analyze libraries of each of the **B-*N*Hep** conjugates (Fig. 3). In addition to its widespread use as a protein and peptide visualization tool, there also is precedence of SDS-PAGE use with complex DCC systems.[9,11,41,44] We examined differences in speciation of the **B-*N*Hep** DCLs containing different length peptides, along with the **B-2.5Hep-Def** (unable to form coiled coils) and **Ac-3Hep** (lacking covalent linkages from the DCC monomer) controls. Libraries of each peptide length were set up at 150 μM, the same concentration used for the LC-MS.

As seen in Fig. 3, a number of discrete species were visualized on the gel that were not resolved in the LC-MS traces.

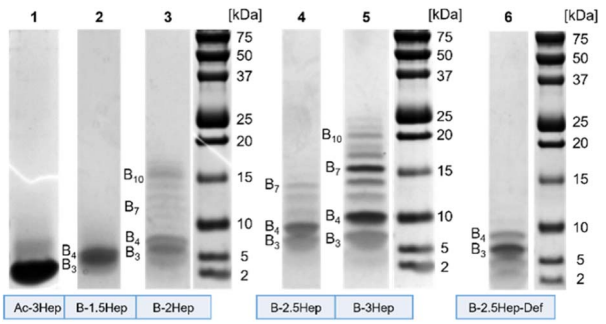

Fig. 3 Bis-Tris SDS-PAGE analysis of libraries of monomer **B** with varying peptide length (**B-1.5Hep-3Hep**) set up at 150 μM, shown in order of increasing heptad length. **Ac-3Hep** was also included as a mass reference. Gels were stained with Coomassie Blue for visualization.

Libraries showed a significant number of higher mass species beyond B_3 and B_4, excepting the **B-1.5Hep** and **B-2.5Hep-Def** libraries (Fig. 3, lane 2 and 6). In accordance with the LC-MS trace, the **B-1.5Hep** libraries exhibit two poorly resolved bands in the gel, corresponding in mass to the B_3 and B_4 species (Table S7†). This indicates that the 1.5-heptad peptides, which are expected to have the weakest coiled coil interactions, have little impact on speciation of the DCL. The intensity of these bands and their relatively small (1524.6 Da) mass difference makes it difficult to distinguish, but the two separate bands can be seen more clearly at lower concentrations (Fig. S31,† lane 1–3; Fig. S32,† lane 3). Similarly, the **B-2.5Hep-Def** library also results in bands for only B_3 and B_4, with a more intense band for B_3, in agreement with the results from LC-MS and MALDI analysis. These controls support the importance of coiled coil formation for the emergence of higher mass species.

Samples of **B-2Hep**, **B-2.5Hep**, and **B-3Hep** monomers (Fig. 3, lanes 3, 4, 5, respectively) display multiple bands corresponding to higher mass species in addition to the trimers (B_3) and tetramers (B_4) favored by unmodified monomer **B**. Thus, coiled coil formation appears to overcome the entropic restriction to smaller rings. Moreover, different numbers and patterns of bands were observed depending on the peptide length. The **B-2Hep** library (Fig. 3, lane 3) shows preferential formation of a species around the B_{10} mass in addition to B_3 and B_4, while the **B-2.5Hep** library (Fig. 3, lane 4) favors B_4 over B_3 and exhibits a significant B_7 band. The **B-3Hep** library (Fig. 3, lane 5) more strongly favors the formation of higher mass species than libraries of other monomers, with a significant preference for B_4, B_7, and to a lesser extent, B_6, B_8, and B_{10}. The **Ac-3Hep** peptide, which cannot form covalent linkages, exhibits an intense band corresponding to the monomeric peptide (2522.4 Da; Fig. 3, lane 1).

The effect of concentration on this speciation pattern was analyzed by equilibrating libraries at varied concentrations (Fig. S31 and S32†). Overall, changing the monomer concentration over a range of 50 μM up to 675 μM did not cause significant changes in speciation or relative abundance beyond a slight increase in higher mass band intensity for the highest concentration libraries (Fig. S31, lanes 1, 5, 9, 13; S32,† lanes 1, 4, 7, 10). Given that coiled coil formation is concentration-dependent,[2] this slight difference is expected. Consistent with the MALDI data, the **B-2.5Hep-Def** libraries showed faint bands for B_5–B_7 in addition to intense bands for B_3 and B_4 when equilibrated at the highest concentration (Fig. S32,† lane 13). However, in contrast to all **B-*N*Hep** DCLs designed to form coiled coils, **B-2.5Hep-Def** does not exhibit preferential formation of any specific higher mass species. In sum, the SDS-PAGE analysis demonstrates that coiled coil formation perturbs the speciation of the DCLs in a length-dependent manner and drives formation of higher-mass oligomers.

Speciation is thermodynamically controlled

We considered the fact that B_7 could be formed by the reaction of a B_3 species with a B_4 species, resulting from a kinetic preference rather than representing an equilibrium mixture. To evaluate whether the speciation of the libraries represents equilibrium or a kinetic trap, a re-equilibration experiment was performed using a 360 μM **B-2.5Hep** library which had previously equilibrated for over a month. 10 mol% TCEP relative to total monomer concentration was added to partially reduce the library. The library was then allowed to re-equilibrate for one week, and both parent and re-equilibrated samples were analyzed by gel electrophoresis (Fig. 4). Comparing the parent and re-equilibrated library samples (Fig. 4, lanes 1 and 2 respectively), the speciation and abundance are virtually identical, indicating that the higher mass species shown are in fact thermodynamically favored products and that the libraries in this study are fully equilibrated.

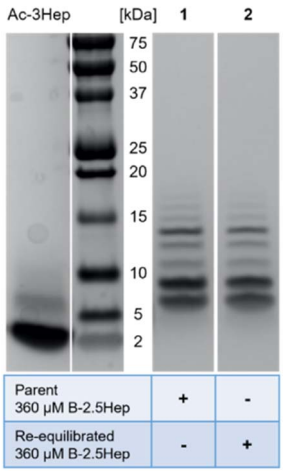

Fig. 4 Bis-Tris SDS-PAGE analysis of the parent (lane 1) and re-equilibrated (partially reduced with 10mol% TCEP and allowed to re-equilibrate; lane 2) 360 μM **B-2.5Hep** library. **Ac-3Hep** peptide was included as a mass standard. Gels were stained with Coomassie Blue for visualization.

Denaturing conditions confirm that the higher mass species are covalent oligomers

While the SDS in Bis-Tris gels is denaturing, we wanted to ensure that all noncovalent interactions in the libraries were fully disrupted and that the larger mass species are covalent oligomers. To do this, we compared our standard gel system (Bis-Tris SDS-PAGE; Fig. S33b†) to a gel containing 6 M urea (Fig. S33a†), which has previously been shown to be an effective denaturing agent for a variety of parallel, dimeric coiled coils.[45–47] Additionally, our own CD analysis showed that adding 6 M urea thoroughly eliminated coiled coil formation for 150 μM **B-2.5Hep** and **Ac-3Hep** library samples (Fig. S34, Table S8†). The addition of 6 M urea to the gel did not cause any significant changes to the number or resolution of bands compared to our standard conditions, further validating that the higher mass species are covalent oligomers.

Cyclic oligomers are formed

To confirm that these higher-mass species are cyclic, as has been observed in other DCLs using dithiols, we treated

equilibrated libraries with 5-iodoacetamidofluorescein (5-IAF), a fluorescent tag capable of reacting with any remaining free thiol. Any acyclic oligomers would contain two thiols that would react with 5-IAF, resulting in both a shift in the mass of the oligomer and a fluorescent signal for bands corresponding to these species on a gel. In comparison, a cyclic macrocycle would not contain any free thiols and would not react with 5-IAF, leaving the library unchanged. We thus compared the fluorescence tagging of a library of **B-2.5Hep** with 5-IAF to a control without added 5-IAF (Fig. 5). We also compared the results to several other controls, including **B-2.5Hep-Def**, reduced **B-2.5Hep**, and an equilibrated **B-2.5Hep** library with added oxidant (sodium perborate).

All 5-IAF labeling experiments utilized equilibrated 450 μM **B-2.5Hep** and **B-2.5Hep-Def** libraries which were then diluted to a concentration of 360 μM library with the addition of 90 μM 5-IAF (0.25 equivalents). Incubation of the library with 5-IAF did not cause any measurable shifts in the bands in the Coomassie-stained gel as compared to libraries without 5-IAF (Fig. 5, lanes 1 *vs.* 2 and 5 *vs.* 6), suggesting that the bands that correspond to $\mathbf{B_3}$ and larger ring sizes are cyclic and thus unreactive toward 5-IAF. The comparison between lanes 1, 2, 5 and 6 also reveals that **B-2.5Hep** and **B-2.5Hep-Def** libraries respond similarly to the addition of 5-IAF, indicating that closed macrocycles form regardless of the presence of coiled coils (Fig. 5c). Fluorescence imaging does not show labeling of any higher mass species. The 5-IAF control sample exhibits two fluorescence bands at low molecular weights (~1.5 kDa and 4 kDa, Fig. 5b and c, lane 7). These same two bands are the only fluorescent bands observed when 5-IAF is mixed with **B-2.5Hep** or **B-2.5Hep-Def** (Fig. 5, lanes 2, 4, and 6) indicating that none of the **B-2.5Hep** species are labeled.

As positive and negative controls, we also investigated the labeling of a reduced library (Fig. 5, lane 3) and an "oxidized" library, in which sodium perborate was added after equilibration in air to ensure that the library was fully oxidized (Fig. 5, lane 4). The reduced sample contained 2.1 equiv. TCEP, while the fully oxidized library contained 2.1 equiv. sodium perborate. An overlay of the Coomassie-stained and fluorescent-imaged gels demonstrates that the reduced library (Fig. 5, lane 3) contains labeled species at low molecular weight that are not seen in standard conditions or in the 5-IAF control (Fig. 5, lane 7). Interestingly, a band for $\mathbf{B_3}$ is also apparent, suggesting rapid re-oxidation to $\mathbf{B_3}$ after reduction with TCEP. In contrast, the oxidized library (Fig. 5, lane 4) looks identical to the equilibrated libraries with or without 5-IAF (Fig. 5, lanes 1 and 2), further supporting that those libraries were fully oxidized and contain only cyclic species.

To further validate these results, we analyzed the libraries corresponding to the standard conditions (Fig. 5, lane 2), reduced library (positive control; Fig. 5, lane 3), and oxidized library (negative control; Fig. 5, lane 4) by LC-MS (Fig. S35†). The LC-MS traces of the oxidized and standard libraries were nearly identical with no identifiable masses corresponding to new 5-IAF labeled oligomers (Fig. S35a and c†), consistent with the Coomassie-stained and fluorescent imaged gels showing no labeling by 5-IAF (Fig. 5, lanes 1 and 2). The LC-MS trace of the reduced sample shows a mixture of unlabeled, 5-IAF-monolabeled, and 5-IAF-dilabeled monomer (Fig. S35b†), consistent with expectations based on the 0.25 equivalents of 5-

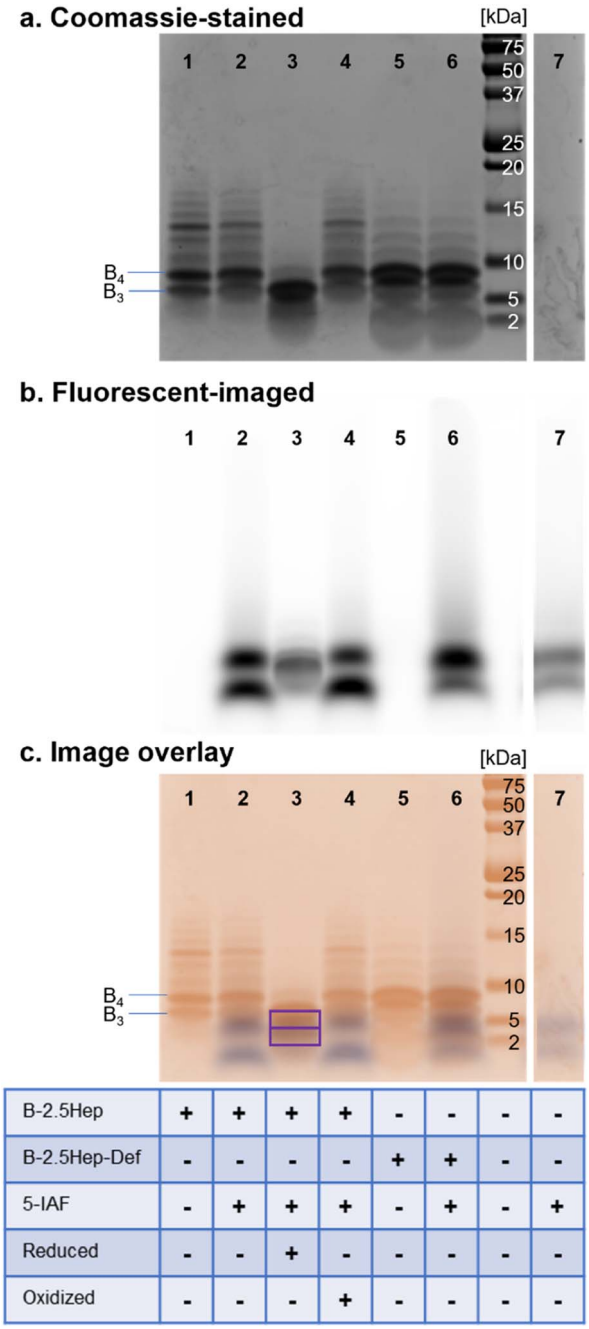

B-2.5Hep	+	+	+	+	-	-	-	-
B-2.5Hep-Def	-	-	-	-	+	+	-	-
5-IAF	-	+	+	+	-	+	-	+
Reduced	-	-	+	-	-	-	-	-
Oxidized	-	-	-	+	-	-	-	-

Fig. 5 Bis-Tris SDS-PAGE analysis of the **B-2.5Hep** and **B-2.5Hep-Def** 450 μM libraries following reaction with 5-IAF. Gels were visualized using (a) Coomassie blue stain and (b) fluorescent-imaging (c) overlay of Coomassie-stained (orange, top) and fluorescent (blue, bottom) images of SDS-PAGE analysis of **B-2.5Hep** and **B-2.5Hep-Def** libraries following reaction with 5-IAF. Purple bands are places of overlap (outlined with purple squares), blue bands are fluorescent bands without Coomassie overlap, and orange bands are Coomassie bands without fluorescent overlap. Reduced libraries contained 756 μM TCEP (2.1 equivalents), while oxidized libraries 756 μM sodium perborate (2.1 equivalents).

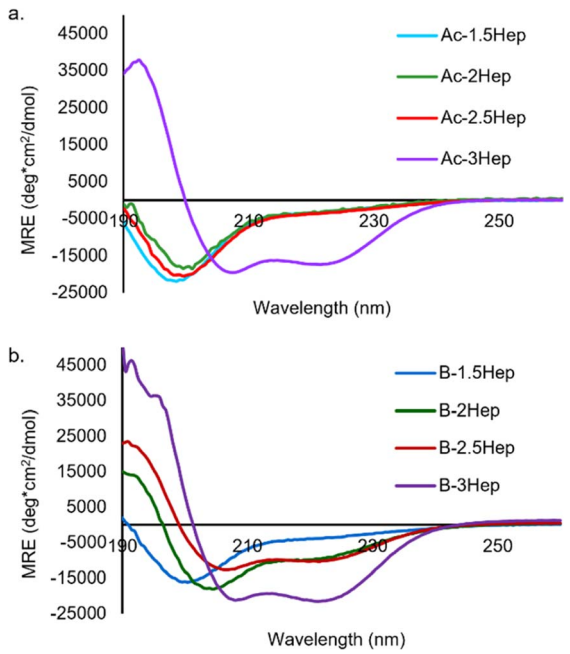

Fig. 6 (a) CD spectra of acetylated coiled coil peptides. (b) CD spectra of B-*N*Hep libraries. Concentration of peptide is 150 mM, 50 mM borate buffer, pH 8.5. Spectra measured at 20 °C.

IAF used and the appearance of overlapping Coomassie-labeled and fluorescent bands on the gel (Fig. 5, lane 3). Taken together, these results show that the oligomers observed in these **B-*N*Hep** libraries do not possess free thiol groups. This indicates that large discrete macrocycles with up to 13 subunits are formed.

Effect of salt on oligomerization. Individual coiled coils are driven by a combination of hydrophobic and electrostatic interactions. To evaluate the contributions of these two types of interactions to macrocycle formation, **B-2.5Hep** and **B-2.5Hep-Def** libraries were equilibrated in sodium borate buffer with and without 100 mM NaCl. SDS-PAGE analysis shows an increase in higher order species with the addition of salt (Fig. S36†). Interestingly, the **B-2.5Hep** library maintains similar speciation patterns as with low salt (Fig. S36,† lanes 1 and 2), suggesting that, even in more polar solvent, specific coiled coil interactions rather than generic hydrophobic affinity are key. Further, the **B-2.5Hep-Def** libraries showed significantly less higher-mass species than the coiled coil-forming equivalent (Fig. S36,† lanes 3 and 4). These results suggest that stabilizing the hydrophobic interactions in the coiled coils can further increase favorability of large rings by further increasing the contribution of the coiled coil formation.

Characterization of DCLs by circular dichroism (CD) spectroscopy

The importance of coiled coil formation on speciation has been suggested by all analyses. Thus, we used CD to characterize the extent of coiled coil formation in the DCLs, as monomeric peptides adopt a random coil conformation whereas binding induces a helical structure, forming a coiled coil. α-Helical coiled coil peptides exhibit a maximum at 190 nm and minima at 208 and 222 nm, whereas random coil structures exhibit a minimum at about 195 nm.[48]

As controls for the **B-*N*Hep** DCLs, we utilized acetyl-capped peptides (**Ac-*N*Hep**) to characterize the degree of coiled coil formation in the absence of a covalent linkage and **Ac-*N*Hep-Def** peptides as negative controls for peptides that cannot form coiled coils. An equilibrated **R-2.5Hep** DCL was used to characterize coiled coil formation with only a single disulfide, which exclusively forms a dimer. Thus, comparing the degree of helicity of **Ac-2.5Hep** to the **R-2.5Hep** dimer and the **B-2.5Hep** DCL correlates with the effect of adding a disulfide linkage and forming a macrocycle, respectively.

As expected, **Ac-3Hep-Def** CD analysis shows a random coil minimum at 198 nm (Fig. S37†). Analysis of the acetylated peptides shows that only the **Ac-3Hep** is able to form coiled coils at 150 μM, whereas the shorter acetylated peptides remain unfolded as random coils, as expected (Fig. 6a).[43] The 4-residue difference between the **Ac-2.5Hep** and **Ac-3Hep** appears to have a significant influence on folding under these conditions, in agreement with similar sequences that have previously been reported.[43]

To determine the influence of covalent templation arising from the macrocycles formed *via* DCC on coiled coil formation, we compared the CD spectra of equilibrated **B-*N*Hep** DCLs with the appropriate **Ac-*N*Hep** control peptide (Fig. 6). The **B-*N*Hep** DCLs represent a mixture of species, so the CD spectra represent the average signal arising from the speciation of the library. Comparison of the **B-1.5Hep** to the **Ac-1.5Hep** peptide indicates that covalent templation has little effect on the extent of coiled coil formation at this length (blue lines, Fig. 6a and b), which is consistent with the speciation studies that show that, like unmodified **B**, **B-1.5Hep** forms only $\mathbf{B_3}$ and $\mathbf{B_4}$. However, as the peptide length increases, coiled coil formation is stabilized in the **B-*N*Hep** peptides (Fig. 6b). This is consistent with increased effective molarity of the covalently linked peptides and has been observed in other covalently templated coiled coils.[25,49–56] **B-2.5Hep** exhibits the greatest improvement in folding/binding relative to **Ac-2.5Hep**, indicating that it is the most cooperative at this concentration. In contrast, **B-3Hep** only exhibits a modest increase in folding relative to **Ac-3Hep** because **Ac-3Hep** forms a dimer in the absence of a covalent linkage at this

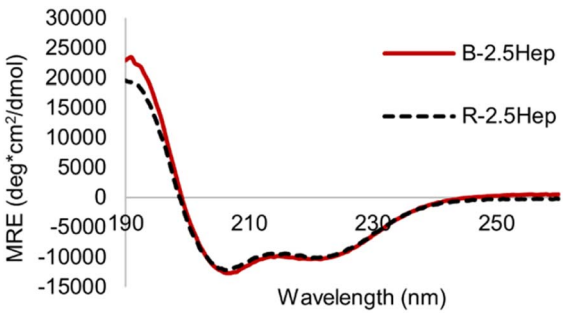

Fig. 7 CD spectrum comparing **R-2.5Hep** and **B-2.5Hep**. Concentration of peptides is 150 μM, scans taken at 20 °C in 50 mM borate buffer, pH 8.5. DCLs were equilibrated for at least 7 days.

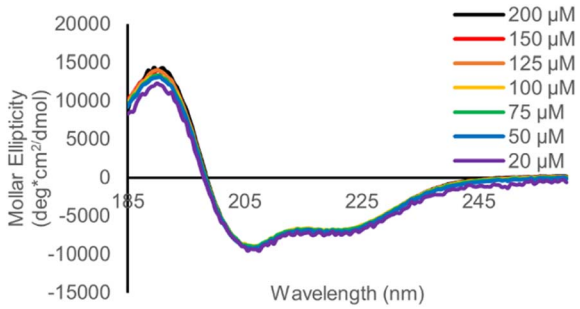

Fig. 8 CD spectrum comparing **B-2.5Hep** from 20–200 μM, demonstrating lack of dependence on concentration. Scans taken at 20 °C in 50 mM borate buffer, pH 8.5. DCLs were equilibrated for at least 7 days.

concentration. As expected, the **B-2Hep-Def** and **B-2.5Hep-Def** samples (Fig. S38 and S39†) remain random coil in the context of the library, indicating that increased effective molarity alone is incapable of inducing coiled coil formation.

To determine whether the formation of macrocycles in **B-*N*Hep** influences the extent of coiled coil formation, we compared the helicity of the **B-2.5Hep** DCL to that of the **R-2.5Hep** disulfide-linked dimer. Overlays of the CD spectra are virtually identical, indicating that the templation effect in the acyclic **R-2.5Hep** dimer is equivalent to that in the mixture of cyclic species formed in the DCL of **B-2.5Hep** (Fig. 7). Importantly, this observation confirms that coiled coil formation is optimized in the DCL.

Taken together, the CD data suggests a scenario in which the magnitude of the coiled coil interaction, as defined by its length, and the effective molarity due to covalent bond formation, are maximized in **B-2.5Hep** to give the greatest improvement in folding due to maximized cooperativity. If the inherent strength of the coiled coil interaction is too low, as in **B-1.5Hep**, the covalent linkage will have little effect and if the coiled coil interaction is too strong, as in **B-3Hep**, the covalent linkage is not necessary to induce folding.

To complement the urea denaturation gel experiments, we measured the concentration dependance of the CD spectrum of **B-2Hep**, **B-2.5Hep** and **R-2.5Hep** from 30–200 mM (Fig. 8, S40, and S41†) to verify that helicity arises from intramolecular interactions. If coiled coil formation is intermolecular, it would be expected to be concentration dependent. However, no change in the CD spectrum was observed, consistent with folding being driven by intramolecular interactions in the **B-*N*Hep** peptides.

Thermal denaturation studies

To evaluate the effect of covalent linkage on the stability of the coiled coil assemblies, thermal denaturation experiments were run on the DCLs by monitoring the MRE signal at 222 nm over a range of temperatures. Melts were performed on **Ac-3Hep**, **B-3Hep**, and **B-2.5Hep**, as each exhibit significant folding at room temperature, as well as the **R-2.5Hep** to compare dimer to oligomer folding. The **B-3Hep** library is the most thermally stable (Fig. 9) with a T_M > 60 °C, which is a ~30 °C shift in T_M relative to **Ac-3Hep**. Interestingly, the **B-3Hep** library appears to exhibit another thermal transition between 5 °C and 35 °C, which may arise from different thermal stabilities of different species in the library. Comparison of the melting curves of **B-2.5Hep** and **R-2.5Hep** indicates that the coiled coil stability of these two libraries is virtually identical (Fig. 9). This suggests that, on average across the species, macrocyclization does not template coiled coil formation any better than the single disulfide bond in the **R-2.5Hep** dimer. Furthermore, the similarity between **Ac-3Hep** and **B-2.5Hep** suggests that covalently linking the 2.5-heptad peptide through disulfide linkages stabilizes the coiled coil approximately as much as adding a half of a heptad in length (Fig. 9).

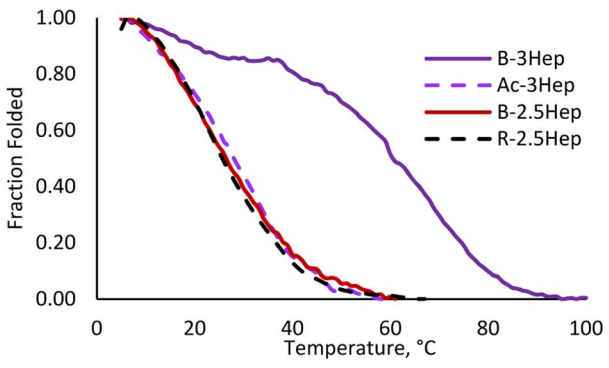

Fig. 9 Melting curve for **Ac-3Hep** (purple dashed), **B-3Hep** (dark purple), **B-2.5Hep** (red), and R-2.5Hep (black dashed). Measurements taken at 222 nm, 150 μM equilibrated samples.

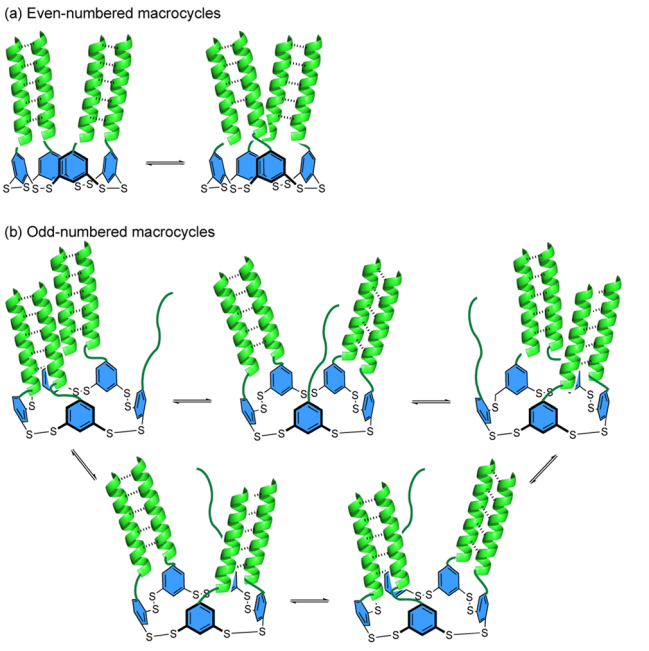

Fig. 10 Cartoon depiction of the proposed dynamic multivalency in macrocycles with (a) even and (b) odd numbers of monomers. Dashed lines show intramolecular coiled coil formation between peptides.

Discussion and conclusions

This investigation demonstrates that an interplay between the mismatched energetic preferences of reversible covalent (a DCC monomer) and noncovalent components (coiled coil peptides) leads to complex behavior. Rather than resulting in the simplest outcome – templation of tetramer $\mathbf{B_4}$ through formation of two coiled coils–the equilibrium is shifted to a series of macrocyclic species from $\mathbf{B_4}$ up to $\mathbf{B_{13}}$, despite the entropic cost of forming larger macrocycles. In addition to $\mathbf{B_4}$, there is also a notable preference for the $\mathbf{B_7}$ macrocycle, which is unexpected as an odd-numbered macrocycle prevents all peptides from having a binding partner. The importance of the coiled coil formation in these species is evident by the significant differences in the abundance and range of higher mass covalent assemblies between the **B-2.5Hep** and **B-2.5Hep-Def** DCLs (Fig. 3), correlating with increased helicity compared to the acetylated control peptides. Concentration dependence studies support that the macrocyclic species are intramolecularly templated. These data, in addition to the fluorescent-labeling experiments (Fig. 5), identify the higher mass species as discrete, internally templated macrocycles.

CD analysis of libraries containing these larger macrocycles does not reveal any significant change to helicity compared to the dimeric **R-*N*Hep** controls (Fig. 7), indicating that the peptides access similar coiled coil dimer structures within the context of the **B-*N*Hep** libraries. The thermal denaturation data indicate increased stability of the coiled coil in **B-*N*Hep** libraries when compared to the corresponding acetylated peptides (Fig. 9) and nearly identical denaturation to the **R-*N*Hep** dimer (Fig. S40†). These data demonstrate that the macrocyclic covalent linkages stabilize the coiled coils due to the higher effective concentration of the peptides from the covalent linkages. However, the similar degree of helicity in the **B-*N*Hep** macrocycles as in the **R-*N*Hep** dimers indicates that formation of higher-mass macrocycles is not driven by an increase in coiled coil formation beyond that of a simple dimer.

As the degree of helicity is no different in the **R-*N*Hep** dimer *versus* **B-*N*Hep** DCL, suggesting that larger macrocycles are not driven by better-templated coiled coils, we considered other factors that may stabilize larger macrocycles. One possibility is that in a small macrocycle, the environment is too crowded or the orientation of the **B**-monomers is unfavorable for optimal coiled coil formation, driving the equilibrium towards larger macrocycles to optimize coiled coils. An additional source of stability may come from dynamic multivalency, which is known to contribute to the binding interactions of some intrinsically disordered proteins.[57–59] In such protein–protein interactions, dynamic multivalency arises when there is more than one degenerate binding epitope that can bind to a single partner protein. Similarly, in **B**-macrocycles reported here, the ability to form multiple degenerate folded states may provide an additional driving force for forming large macrocycles. Coiled coils are known to have rapid folding and unfolding rates.[60] Thus, each peptide likely exists in a rapid equilibrium of dimeric partners with the peptide on either side. This results in increased dynamic multivalency as ring size and peptide components in the ring increase. Making the simplifying assumption that the peptides can only form coiled coils with adjacent peptides and that each coiled coil is energetically identical, this dynamic multivalency results in each macrocycle having at least two enthalpically degenerate states in even-numbered macrocycles, resulting in a more entropically favored assembly (Fig. 10). Odd -numbered rings can exist in more than 2 degenerate states due to the presence of an unpaired peptide (Fig. 10b), increasing their entropic favorability. Furthermore, specific macrocycles may be favored due to optimization of intramolecular interactions within the aromatic core, as it has been shown that such disulfide-linked macrocycles can take on specific folded structures mediated by π–π stacking between the subunits.[33,61,62] Furthermore, cross-macrocycle coiled coils between non-adjacent monomers may also be possible. Together, these combined factors contribute to the increased stability of large macrocycles.

In summary, we describe the coupling of mismatched covalent and noncovalent templation that results in emergent behavior beyond the individual preferences of each component. Although the peptide forms coiled coil dimers, differences in conformational preferences of different ring size that influence interactions between neighboring peptides as well as dynamic exchange between coiled coils within the covalent macrocycle may provide an additional driving force for assembly into larger rings. The size and speciation of the macrocycles correlates with the length, and hence extent of folding and binding, of the coiled coil peptides, resulting in a greater shift towards higher-mass species with more stable coiled coils. Moreover, specific ring sizes are favored over others, presumably due to other conformational preferences. The outcome of this mismatched templation is access to discrete yet complex protein-like assemblies not readily accessible using other methods.[12] The changes in assembly based on heptad length and coiled coil stability suggest a wealth of novel behavior still to be accessed, given the broad array of coiled coil designs that can be incorporated. Work towards exploring this line of inquiry is currently underway.

Data availability

All experimental procedures and characterization data are available in the ESI.†

Author contributions

M. L. W. conceived of the project and obtained funding. K. J. S., B. A. C., and K. M. K. contributed to collecting the data. K. J. S., B. A. C., K. M. K., and M. L. W. contributed to analyzing the data. K. J. S. wrote the original draft of the manuscript. K. M. K and M. L. W. edited the manuscript.

Conflicts of interest

There are no conflicts to declare.

Acknowledgements

We acknowledge funding from NSF grant CHE-2107685 to M. L. W. and NIH grant K12-GM000678 to K. M. K. This work was also supported by the National Cancer Institute of the National Institutes of Health under award number P30CA016086 to support the UNC Macromolecular Interactions Facility. We thank Brandie Ehrmann and E. Diane Weatherspoon in the University of North Carolina's Department of Chemistry Mass Spectrometry Core Laboratory for their assistance with mass spectrometry analysis. We thank Dr Ashutosh Tripathy for assistance with CD.

Notes and references

1 A. R. Thomson, C. W. Wood, A. J. Burton, G. J. Bartlett, R. B. Sessions, R. L. Brady and D. N. Woolfson, *Science*, 2014, **346**, 485–488.
2 D. N. Woolfson, in *Fibrous Proteins: Structures and Mechanisms*, ed. D. A. D. Parry and J. M. Squire, Springer International Publishing, Cham, 2017, pp. 35–61.
3 J. M. Fletcher, A. L. Boyle, M. Bruning, G. J. Bartlett, T. L. Vincent, N. R. Zaccai, C. T. Armstrong, E. H. C. Bromley, P. J. Booth, R. L. Brady, A. R. Thomson and D. N. Woolfson, *ACS Synth. Biol.*, 2012, **1**, 240–250.
4 A. L. Boyle and D. N. Woolfson, *Chem. Soc. Rev.*, 2011, **40**, 4295–4306.
5 J. M. Fletcher, K. A. Horner, G. J. Bartlett, G. G. Rhys, A. J. Wilson and D. N. Woolfson, *Chem. Sci.*, 2018, **9**, 7656–7665.
6 D. N. Woolfson, *J. Mol. Biol.*, 2021, **433**, 167160.
7 W. M. Rink and F. Thomas, *Chem. - Eur. J.*, 2019, **25**, 1665–1677.
8 I. V. Korendovych and W. F. DeGrado, *Q. Rev. Biophys.*, 2020, **53**, e3.
9 T. D. Samdin, A. G. Kreutzer and J. S. Nowick, *Curr. Opin. Chem. Biol.*, 2021, **64**, 106–115.
10 S. Haerianardakani, A. G. Kreutzer, P. J. Salveson, T. D. Samdin, G. E. Guaglianone and J. S. Nowick, *J. Am. Chem. Soc.*, 2020, **142**, 20708–20716.
11 S. Zhang, S. Yoo, D. T. Snyder, B. B. Katz, A. Henrickson, B. Demeler, V. H. Wysocki, A. G. Kreutzer and J. S. Nowick, *Biochemistry*, 2022, **61**, 252–264.
12 F. Sheehan, D. Sementa, A. Jain, M. Kumar, M. Tayarani-Najjaran, D. Kroiss and R. V. Ulijn, *Chem. Rev.*, 2021, **121**, 13869–13914.
13 M. Nepal, M. J. Sheedlo, C. Das and J. Chmielewski, *J. Am. Chem. Soc.*, 2016, **138**, 11051–11057.
14 M. Nambiar, L.-S. Wang, V. Rotello and J. Chmielewski, *J. Am. Chem. Soc.*, 2018, **140**, 13028–13033.
15 J. M. Galloway, H. E. V. Bray, D. K. Shoemark, L. R. Hodgson, J. Coombs, J. M. Mantell, R. S. Rose, J. F. Ross, C. Morris, R. L. Harniman, C. W. Wood, C. Arthur, P. Verkade and D. N. Woolfson, *Small*, 2021, **17**, 2100472.
16 H. Tsutsumi, K. Tanaka, J. Y. Chia and H. Mihara, *Pept. Sci.*, 2021, **113**, e24214.
17 C. Shao, Y. Tian, Z. Dong, J. Gao, Y. Gao, X. Jia, G. Guo, X. Wen, C. Jiang and X. Zhang, *Am. J. Biomed. Sci.*, 2012, **4**, 85–101.
18 J. Wang, C. Wang, Y. Ge, Y. Sun, D. Wang and H. Xu, *Pept. Sci.*, 2021, **113**, e24208.
19 K. S. Hellmund, B. von Lospichl, C. Böttcher, K. Ludwig, U. Keiderling, L. Noirez, A. Weiß, D. J. Mikolajczak, M. Gradzielski and B. Koksch, *Pept. Sci.*, 2021, **113**, e24201.
20 R. S. Giri, S. Pal, S. Roy, G. Dolai, S. R. Manne, S. Paul and B. Mandal, *Pept. Sci.*, 2021, **113**, e24176.
21 H. E. Distaffen, C. W. Jones, B. L. Abraham and B. L. Nilsson, *Pept. Sci.*, 2021, **113**, e24224.
22 J. N. Sloand, M. A. Miller and S. H. Medina, *Pept. Sci.*, 2021, **113**, e24184.
23 R. W. Curtis and J. Chmielewski, *Pept. Sci.*, 2021, **113**, e24190.
24 H. Jędrzejewska, M. Wierzbicki, P. Cmoch, K. Rissanen and A. Szumna, *Angew. Chem., Int. Ed.*, 2014, **53**, 13760–13764.
25 M. Mutter and S. Vuilleumier, *Angew. Chem., Int. Ed. Engl.*, 1989, **28**, 535–554.
26 J. O. Freeman, W. C. Lee, M. E. P. Murphy and J. C. Sherman, *J. Am. Chem. Soc.*, 2009, **131**, 7421–7429.
27 P. T. Corbett, J. Leclaire, L. Vial, K. R. West, J.-L. Wietor, J. K. M. Sanders and S. Otto, *Chem. Rev.*, 2006, **106**, 3652–3711.
28 M.-K. Chung, P. S. White, S. J. Lee, M. R. Gagné and M. L. Waters, *J. Am. Chem. Soc.*, 2016, **138**, 13344–13352.
29 M.-K. Chung, P. S. White, S. J. Lee, M. L. Waters and M. R. Gagné, *J. Am. Chem. Soc.*, 2012, **134**, 11415–11429.
30 M.-K. Chung, S. J. Lee, M. L. Waters and M. R. Gagné, *Chem. Commun.*, 2016, **52**, 8103–8106.
31 M.-K. Chung, S. J. Lee, M. L. Waters and M. R. Gagné, *J. Am. Chem. Soc.*, 2012, **134**, 11430–11443.
32 C. G. Pappas, B. Liu, I. Marić, J. Ottelé, A. Kiani, M. L. van der Klok, P. R. Onck and S. Otto, *J. Am. Chem. Soc.*, 2021, **143**, 7388–7393.
33 C. G. Pappas, P. K. Mandal, B. Liu, B. Kauffmann, X. Miao, D. Komáromy, W. Hoffmann, C. Manz, R. Chang, K. Liu, K. Pagel, I. Huc and S. Otto, *Nat. Chem.*, 2020, **12**, 1180–1186.
34 Y. Altay, M. Tezcan and S. Otto, *J. Am. Chem. Soc.*, 2017, **139**, 13612–13615.
35 B. Liu, C. G. Pappas, E. Zangrando, N. Demitri, P. J. Chmielewski and S. Otto, *J. Am. Chem. Soc.*, 2019, **141**, 1685–1689.
36 M. Malakoutikhah, J. J.-P. Peyralans, M. Colomb-Delsuc, H. Fanlo-Virgós, M. C. A. Stuart and S. Otto, *J. Am. Chem. Soc.*, 2013, **135**, 18406–18417.
37 B. Bartolec, M. Altay and S. Otto, *Chem. Commun.*, 2018, **54**, 13096–13098.
38 G. Wołczański, M. Cal, M. Waliczek, M. Lisowski and P. Stefanowicz, *Chem. - Eur. J.*, 2018, **24**, 12869–12878.
39 L. Roy and M. A. Case, *J. Am. Chem. Soc.*, 2010, **132**, 8894–8896.
40 J. M. A. Carnall, C. A. Waudby, A. M. Belenguer, M. C. A. Stuart, J. J.-P. Peyralans and S. Otto, *Science*, 2010, **327**, 1502–1506.

41 J. Li, J. M. A. Carnall, M. C. A. Stuart and S. Otto, *Angew. Chem., Int. Ed.*, 2011, **50**, 8384–8386.
42 L. Roy and M. A. Case, *J. Phys. Chem. B*, 2011, **115**, 2454–2464.
43 F. Thomas, A. L. Boyle, A. J. Burton and D. N. Woolfson, *J. Am. Chem. Soc.*, 2013, **135**, 5161–5166.
44 J. F. Reuther, J. L. Dees, I. V. Kolesnichenko, E. T. Hernandez, D. V. Ukraintsev, R. Guduru, M. Whiteley and E. V. Anslyn, *Nat. Chem.*, 2018, **10**, 45–50.
45 O. D. Monera, N. E. Zhou, C. M. Kay and R. S. Hodges, *J. Biol. Chem.*, 1993, **268**, 19218–19227.
46 O. D. Monera, C. M. Kay and R. S. Hodges, *Protein Sci.*, 1994, **3**, 1984–1991.
47 H. Gradišar and R. Jerala, *J. Pept. Sci.*, 2011, **17**, 100–106.
48 M. D. Bruch, M. M. Dhingra and L. M. Gierasch, *Proteins: Struct., Funct., Bioinf.*, 1991, **10**, 130–139.
49 M. G. Wuo, A. B. Mahon and P. S. Arora, *J. Am. Chem. Soc.*, 2015, **137**, 11618–11621.
50 M. G. Wuo, S. H. Hong, A. Singh and P. S. Arora, *J. Am. Chem. Soc.*, 2018, **140**, 16284–16290.
51 L. K. Henchey, A. L. Jochim and P. S. Arora, *Curr. Opin. Chem. Biol.*, 2008, **12**, 692–697.
52 P. E. Dawson and S. B. H. Kent, *J. Am. Chem. Soc.*, 1993, **115**, 7263–7266.
53 M. Mutter, P. Dumy, P. Garrouste, C. Lehmann, M. Mathieu, C. Peggion, S. Peluso, A. Razaname and G. Tuchscherer, *Angew. Chem., Int. Ed. Engl.*, 1996, **35**, 1482–1485.
54 B. Dang, H. Wu, V. K. Mulligan, M. Mravic, Y. Wu, T. Lemmin, A. Ford, D.-A. Silva, D. Baker and W. F. DeGrado, *Proc. Natl. Acad. Sci. U. S. A.*, 2017, **114**, 10852–10857.
55 A. J. Doerr and G. L. McLendon, *Inorg. Chem.*, 2004, **43**, 7916–7925.
56 M. L. Zastrow and V. L. Pecoraro, *Coord. Chem. Rev.*, 2013, **257**, 2565–2588.
57 J. Weng and W. Wang, *Curr. Opin. Struct. Biol.*, 2020, **62**, 9–13.
58 L. M. Stevers, P. J. de Vink, C. Ottmann, J. Huskens and L. Brunsveld, *J. Am. Chem. Soc.*, 2018, **140**, 14498–14510.
59 H. W. Ooi, J. M. M. Kocken, F. L. C. Morgan, A. Malheiro, B. Zoetebier, M. Karperien, P. A. Wieringa, P. J. Dijkstra, L. Moroni and M. B. Baker, *Biomacromolecules*, 2020, **21**, 2208–2217.
60 H. Chao, E. Houston Michael, S. Grothe, C. M. Kay, M. O'Connor-McCourt, R. T. Irvin and R. S. Hodges, *Biochemistry*, 1996, **35**, 12175–12185.
61 L. Vial, F. Perret and J. Leclaire, *Eur. J. Org. Chem.*, 2022, **2022**, e202101274.
62 P.-T. Skowron, M. Dumartin, E. Jeamet, F. Perret, C. Gourlaouen, A. Baudouin, B. Fenet, J.-V. Naubron, F. Fotiadu, L. Vial and J. Leclaire, *J. Org. Chem.*, 2016, **81**, 654–661.